Repopulated microglia induce expression of Cxcl13 with modest changes in Tau phosphorylation but do not impact amyloid pathology

M. Kerry O'Banion (kerry_obanion@urmc.rochester.edu)
University of Rochester School of Medicine & Dentistry
Berke Karaahmet
University of Rochester School of Medicine & Dentistry
Linh Le
University of Rochester School of Medicine & Dentistry
Monique S. Mendes
University of Rochester School of Medicine & Dentistry
Ania K. Majewska
University of Rochester School of Medicine & Dentistry

Research Article

Keywords: Alzheimer's Disease, Colony-stimulating factor 1, PLX5622, microglia, RNAseq

Posted Date: March 14th, 2022

DOI: https://doi.org/10.21203/rs.3.rs-1435003/v1

Abstract

Background: Adult microglia rely on self-renewal through division to repopulate and sustain their numbers. However, with aging, microglia display morphological and transcriptional changes that reflect a heightened state of neuroinflammation. This state threatens aging neurons and other cells and can influence the progression of Alzheimer's disease (AD). In this study, we sought to determine whether renewing the microglia through a forced partial depletion/repopulation method could attenuate AD pathology in the 3xTg and APP/PS1 mouse models.

Methods: We pharmacologically depleted the microglia of two cohorts of 21-22 month old 3xTg mice and one cohort of 14 month old APP/PS1 mice using PLX5622 formulated in chow for 2 weeks. Following depletion, we returned the mice to standard chow diet for 1 month to allow microglial repopulation. We assessed the effect of depletion and repopulation on AD pathology, microglial gene expression, and surface expression of homeostatic markers on microglia using immunohistochemistry, single-cell RNAseq and flow cytometry.

Results: Although we did not identify a significant impact of microglial repopulation on amyloid pathology in either of the AD models, we observed a modest but significant increase in specific isoforms of phosphorylated-Tau species after repopulation in the 3xTg mice. We provide evidence that repopulated microglia in the hippocampus exhibited changes in the expression of homeostatic microglial markers. Lastly, we identified novel subpopulations of microglia by performing single-cell RNAseq analysis on $CD45^{int/+}$ cells from hippocampi of control and repopulated 3xTg mice. In particular, one subpopulation induced after repopulation is characterized by heightened expression of *Cxcl13*.

Conclusion: Overall, we found that depleting and repopulating microglia alters their phenotype and causes overexpression of microglial *Cxcl13* with disparate effects on Tau and amyloid pathologies.

Introduction

Microglia are the brain's immune cells and are critical for normal brain function. In addition to their roles in maintaining tissue homeostasis, they are also key players in the pathogenesis and progression of Alzheimer's disease (AD). Neuroinflammation associated with microglial changes is a cardinal feature of AD and leads to increased Tau pathology and hippocampal dysfunction (1–3). Molecular mechanisms of the microglial response to AD pathology and the heterogeneity of microglial phenotypes in AD brains are the subject of intense debate. Several studies have identified a transcriptionally characterized cluster of microglia induced by aging and multiple neurodegenerative diseases, including AD, commonly referred to as disease associated microglia (DAM) (4–8). This cluster is defined by reduced expression of microglial homeostatic genes such as *Cx3cr1, P2ry12*, and *Tmem119* with concomitant upregulation of genes associated with lysosomal phagocytic activity and lipid metabolism such as *Apoe, Axl, Csf1, Clec7a, Cst7, Igf1, and Lpl* (4–8), some of which are implicated in AD pathogenesis (8–15). Other clusters of microglia that accompany amyloid pathology have also been described, such as Interferon Response

Microglia (IRMs) that display upregulation of genes pertinent to interferon pathways (14, 16). Although advances in single-cell RNA sequencing (scRNAseq) technologies have enabled the discovery of many novel clusters of microglia in homeostasis or disease, the full extent of microglial heterogeneity and its relationship to spatiotemporal properties of AD is still unclear.

To test whether microglia can alter AD pathogenesis, investigators have depleted microglia in the diseased brain using multiple techniques (17). Recently, rapid partial depletion of microglia through oral administration of antagonists to Colony-Stimulating-Factor-1-Receptor (CSF1R) signaling, which plays a role in microglial maintenance, has been widely utilized (18–21). In the 5xFAD model of AD, inflammatory gene expression in the hippocampus was reversed with continuous depletion of microglia in aged mice, along with reduced neuritic damage and better performance on memory tests (19). In aged 3xTg mice, sustained low-dose CSF1R inhibition of microglia showed an association between removal of microglia around amyloid-beta (Aβ) plaques and improved cognitive outcomes (18). However, the effects of microglia elimination on amyloid plaque burden remain controversial, with data supporting no change (18, 19), exacerbation (22), or amelioration of amyloid pathology (20, 21). Similarly, the impact of depletion on Tau pathology has been variable, perhaps due to the innate characteristics of the models used. Taken together, these findings reinforce the notion that microglia play active roles in AD, and depletion leads to variable changes during AD pathogenesis.

Adult microglia have a remarkable capacity to self-renew, and after depletion, repopulate their niche completely within one week, acquiring their normal densities, spacing, and morphological characteristics (23–27). A number of studies have reported that depleting and repopulating microglia changes their phenotype to various degrees (28–30). Here, we partially depleted microglia within the AD brain with PLX5622, a CSF1R inhibitor, and then allowed microglia to repopulate in order to investigate whether renewing microglia through this method could affect cognitive deficits, plaque formation, and Tau hyperphosphorylation in two mouse models of AD. While we observed changes in homeostatic markers in repopulated microglia, we did not see any differences in behavior between control and repopulated 3xTg mice. Microglial repopulation did not alter microglial phagocytosis of Aβ or amyloid plaque burden in either 3xTg or APP/PS1 mice. The impact of microglial renewal on Tau pathology was complex, with different Tau epitopes exhibiting different changes in phosphorylation. Interestingly, we found a novel enriched subpopulation of repopulated microglia characterized by upregulation of *Cxcl13.* CXCL13 is a small chemokine that can regulate lymphocyte homing and plays an important role in lymphoid neogenesis (31–33). We visualized its expression in regions associated with AD pathology in PLX-treated 3xTg mice; however, the biological significance of *Cxcl13* requires further investigation. Overall, our data suggest that repopulation of microglia after partial depletion induces a novel microglial phenotype that is correlated with variable changes in Tau phosphorylation.

Methods

Experimental Animals

All animal procedures were reviewed and approved by the University Committee on Animal Resources of the University of Rochester Medical Center and performed according to the Institutional Animal Care and Use Committee and guidelines from the National Institute of Health (NIH). Animals were housed in a 12-hour light/12-hour dark cycle with food *ad libitum*. 14-month-old male and female Tg(APPswe, PSEN1dE9)85Dbo mice (also known as APP/PS1) were obtained from an established colony (JAX stock no. 005864) maintained at the University of Rochester vivarium. Tg(APPSwe, tauP301L)1Lfa $Psen1^{tm1Mpm}$ mice (also known as 3xTg) were initially obtained from Frank M. LaFerla and Salvatore Oddo by Howard Federoff and maintained at the University of Rochester as a homozygous line. The 3xTg mice express mutated human APP Swedish, MAPT P301L under the control of the Thy1.2 promoter and PS1 M146V under the Psen1 promoter. Age-matched non-transgenic (NTg) mice, bred continuously in a parallel colony to 3xTgs with a similar genetic background, were used as wild-type controls to 3xTg mice in RNA sequencing experiments. With age, the 3xTg mice develop Aβ plaque deposits and intraneuronal hyperphosphorylated Tau aggregates. Our studies used two cohorts of 21-22-month-old male 3xTg mice.

Microglia depletion and repopulation

Mice received a chow diet (AIN-76A-D1001i, Research Diets) containing 1200 mg/kg PLX5622 (Chemgood) *ad libitum* for 2 weeks to deplete microglia. Control chow with the same base formula without PLX5622 was given to the control group. After the 2-week treatment, mice were returned to the standard chow diet: AIN-76A (Research Diets) for the 3xTg Cohort 1 or 5053-Rodent Diet 20 (currently in use at the University of Rochester vivarium) for other experiments to allow microglial repopulation for 1 month. All of these formulations were irradiated by the vendor.

Behavioral assays

Open field (OF):

14 days before behavioral testing, mice were switched to a reverse light/dark cycle room. For 2 days before behavioral testing, mice were transported from the colony room to the behavior room, handled for ~5 minutes, and returned to the colony room on that day. On the day of testing, individual mice were placed in the center of a 31x31 cm box. After 20s, the animal's behavior was video recorded for 5 minutes. Mouse entries and time spent in the center zone and outside the zone were quantified using AnyMaze software (Stoelting Co).

Novel Object Recognition (NOR):

For the novel object recognition testing, mice were allowed to freely explore a 31 x 31 cm box containing two identical objects for 10 minutes. Doorknobs (5-6 cm in height and ~3 cm in width) were used. The

testing chamber was sanitized between each trial with 70% ethanol. An hour after the habituation phase, mice were returned to the same box with one of the previously exposed, familiar objects and a novel object (i.e., a different doorknob). Placement of the novel object was randomized for each test. Mice were allowed to explore the box again for 5 minutes. Mice were videotaped during habituation and testing trials. For scoring, the time mice moved toward the object with the head facing the object and the neck extended was counted as exploratory behavior. Mice that spent less than 8 seconds exploring both objects were excluded from the analysis. Novel object discrimination index (DI) was defined by the following formula:

$$Discrimination\ Index = \frac{Tn - Tf}{Tn + Tf}$$

Tf = Time spent with Familiar Object

Tn = Time spent with Novel Object

Lashley Maze:

The Lashley III maze was used to test spatial memory in a stress-free environment (34). The maze consisted of a start box, three interconnected alleys, and a pseudo-home cage. The alley was divided into zones. Mice were allowed to explore the maze for 10 mins per day. The maze was sanitized with 70% ethanol between each trial and each animal. For 8 days, the number of zone entries was recorded under the assumption that mice that correctly remember the route from starting box to the pseudo-home cage will not enter zones outside of the direct path. Anymaze was used to record the videos.

Contextual Fear conditioning (CFC):

After the behavioral tests above were conducted, mice underwent cued and contextual fear conditioning as previously described (35). Briefly, on the conditioning day, mice were allowed to explore the context compromised of an enclosed Plexi-glass chamber and a metal floor grid (model H10-11M, Coulbourn Instruments) inside an isolation chamber (Model H10-24T, Coulbourn Instruments). After 3 min, 15s of white noise was presented, followed by a 2s, 0.75mA foot shock. The noise-shock pairing was repeated twice for a total of 3 shocks with 30s intervals. The next day, mice were exposed to the same chamber for 5 minutes, and freezing behavior was quantified with AnyMaze. Four hours later, the mice were placed in a novel context (a plastic cylinder with bedding and red light) within the same Plexi-glass chamber. After 3 minutes, the conditioned tone stimulus was played, and freezing behavior was quantified.

Flow cytometry / FACS

Mice were injected 24 hours before sacrifice with Methoxy-X04 (MeX04, i.p., 4mg/kg, Tocris Biosciences), a brain-permeable Aβ fluorescent marker (36, 37). On the day of sacrifice, animals were deeply anesthetized with a mixture of xylazine (i.p., 10 mg/kg) and ketamine (i.p., 100 mg/kg) and perfused intracardially with 0.15M phosphate buffer (PB) containing 0.5% sodium nitrite and 2 IU heparin/ml. After perfusion, hemispheres were separated: one was either immediately submerged in fixative solution (4% paraformaldehyde (PFA), pH 7.2 in PB, 4°C) to be used for immunofluorescence experiments or flash-frozen in cold isopentane for ELISA (both as described below), and the other was processed for flow cytometry as follows. The hippocampus from each half brain was dissected and homogenized in 3 ml FACS buffer (1X Phosphate Buffered Saline (PBS) + 0.5% BSA). Homogenates were filtered through a 70 µm cell strainer into a 15 ml tube containing 3 ml FACS buffer. The strainer was washed with an additional 3 ml of FACS buffer, and the cell suspensions were centrifuged at 400xg for 5 min at 4°C. The supernatants were discarded, and the remaining pellets were resuspended in 40% percoll (Cytiva) prepared with PBS, then centrifuged at 400g for 30 min with no braking. After removing the supernatants, the pellets were resuspended in 90 µl FACS buffer with 1:100 Fc block (2.4G2, 1:100, BioLegend) and transferred to a 96 well-plate. After a 15 min incubation with Fc block at 4°C, the following antibodies were added in a 10 µl master mix: CD11b-FITC (M1/70, Biolegend), CD45-APC/Cy7 (30F11, Biolegend), 7AAD (Invitrogen), P2Ry12-APC (S16007D, Biolegend) & TMEM119-PE (106-6, Abcam). The latter two cell surface molecules are considered homeostatic microglial markers (4). The plate was then incubated for 30 mins at 4°C in the dark. The samples were washed once with FACS buffer and transferred to 5 ml tubes containing 7AAD such that its final dilution was 1:80. Appropriate fluorescent-minus-one (FMO) and single-stained bead controls (Ultracomp eBeads, Invitrogen) were prepared in tandem with samples. After excluding debris, doublets, and dead cells, $CD45^{lo}/CD11b^{+}$ was used to gate for microglia on a FACSAria II (BD). $MeX04^{+}$ and $MeX04^{-}$ microglia were sorted. Samples from APP/PS1 mice were analyzed the same way, but with a LSR II flow cytometer (BD) without sorting. All events were recorded, and data were analyzed with FCS Express 7 (DeNovo Software).

Immunofluorescence

Half-brains were fixed overnight in 4% PFA at 4°C, dehydrated in 30% sucrose overnight, frozen in cold isopentane, and stored at -80°C until sectioning on a -25°C freezing stage microtome into 30 µm thick coronal slices stored in cryoprotectant solution. For immunofluorescence, sections were washed extensively in PBS and blocked with 10% normal donkey or goat serum for 1 h at RT.

For amyloid pathology analysis, sections were immunolabeled for amyloid-beta (Aβ), microglia (Iba1 or P2RY12), a common microglial activation marker CD68, and a widely-used marker for neuritic damage LAMP1 (38). The following primary antibodies were used: biotin anti-Aβ (clone 6E10, 1:3000, BioLegend), rabbit anti-Iba1 (1:2000, Wako), rabbit anti-P2RY12 (1:2000, Anaspec), rat anti-CD68 (1:500, Bio-Rad) and rat anti-LAMP1 (1:2000, Abcam). Sections were incubated in primary antibodies for 48 h at 4°C. The

sections were washed and incubated in fluorescently-labeled secondary antibodies/reagents (Alexa Fluor 488, Alexa Fluor 594 streptavidin conjugate and Alexa Fluor 647, Invitrogen; all at 1:1000) for 3 h at RT, then mounted and coverslipped (Prolong Gold, ThermoFisher Scientific).

For Tau pathology analysis, sections were incubated in biotinylated mouse anti-HT7 (1:1000, Invitrogen) and either rabbit anti-pT205 (1:1000, Invitrogen) or rabbit anti-pS396 (1:1000, RayBiotech) for 2 h at RT then overnight at 4°C. They were washed, incubated in fluorescently-labeled secondary antibodies (Alexa Fluor 488, Invitrogen) and Alexa fluor 594 streptavidin conjugate (Invitrogen; all at 1:1000) for 3 h at RT, and then mounted and coverslipped.

Image acquisition and analysis

For each animal, 3-4 coronal tissue sections that included the subiculum (S) and CA1 field of the hippocampus (CA1) were imaged with a Nikon A1R HD confocal microscope using a 10x (Plan Apo Lambda, NA: 0.40), 20x (Plan Apo VC, NA: 0.75) or 40x water-submersion (Apo LWD, NA: 1.15) objective lens as indicated in figure legends. Imaging parameters were kept constant across all sections for each set of immunofluorescent labels. All image analysis was performed using ImageJ FIJI (NIH) with semi-automated custom macros. Experimenters were blinded to treatment.

Analysis of amyloid pathology and associated neuritic damage

For plaque area fraction and number analysis, regions of interest (ROIs) outlining the above-mentioned structures (S and CA1 for APP/PS1 and S for 3xTg) were drawn on maximum z-projections of the acquired 6E10 images. Images were subsequently thresholded and binarized using automated ImageJ's Otsu thresholding algorithm, which was used for all other thresholding steps in this manuscript (except for MeX04 analysis, in which MaxEntropy was used). The plaque area fraction was calculated as the ratio between the number of pixels above the threshold over all pixels in the ROIs. The number of plaques per ROI was computed using automated ImageJ's analyze particles function with a cut-off size of 50 μm^2.

For quantification of plaque-associated neuritic damage, 6E10 z-stacks were thresholded and binarized for analysis taking into account individual z planes. Subsequently, plaques detected by the analyze particles algorithm were dilated 25 µm to encompass the surrounding tissue for quantification of plaque-associated LAMP1. The overlap between LAMP1 and microglia was measured by multiplying the binarized LAMP1 and Iba1 (or P2RY12) image stacks. The resultant image was subtracted from the binarized LAMP1 image to obtain a non-microglial LAMP1 image, which was multiplied with the image containing dilated plaques to compute the overlap between LAMP1 and areas surrounding plaques. The number of colocalized signal pixels was calculated and divided by the number of thresholded 6E10 pixels

(non-dilated) to obtain the ratio of LAMP1/plaque as quantification of plaque-associated dystrophic neurites.

Analysis of microglia

To measure the total volume occupied by microglia, Iba1 or P2RY12 z-stacks were thresholded and binarized using the same algorithm as described above. The percentage thresholded pixels was recorded as % microglia coverage. The 6E10 thresholded z-stacks mentioned above were dilated 5 µm, then plaque outlines were overlayed on Iba1 or P2RY12 z-stacks. The percentage of microglial area associated with plaque was calculated as the number of colocalized signal pixels divided by all microglial pixels.

To assess microglial activation, CD68 and P2RY12 markers were quantified. CD68 analysis was performed on APP/PS1 and the first cohort of 3xTg animals, while P2RY12 analysis was done on the second 3xTg cohort. CD68 z-stacks were thresholded and binarized within the same region. The overlap between CD68 and microglia was measured by multiplying the binarized CD68 and Iba1 z-stacks. The number of colocalized signal pixels was divided by the total microglia pixels to get the fraction of CD68-expressing microglia. For quantification of P2RY12 intensity as a proxy for microglia activation state, P2RY12 slices were summed in the z-direction and duplicated. One P2RY12 image was thresholded, and the P2RY12-negative region was chosen as the background ROI. On the other image, background intensity was measured on the P2RY12 z-sum projection within the pre-defined background ROI. The pixel value for background intensity was then subtracted from the entire image. Subsequently, P2RY12 intensity was measured.

Analysis of Tau pathology

For 3xTg animals that exhibit tauopathy, images containing CA1, the region with the highest accumulation of pathological Tau, were analyzed. The area fraction of total Tau (HT7) and two phospho-Tau epitopes (pT205 and pS396) were computed in a similar manner as described above for plaque analysis. The ratio between pT205 or pS396 and HT7 was calculated and reported.

Single-cell RNA sequencing

Generation of microglia single-cell suspension for sequencing

3xTg control-chow treated, 3xTg PLX-repopulated, and non-transgenic control-chow treated (NTg) mice were perfused and processed as described above in *Flow Cytometry*. All of the equipment was maintained at 4°C, and the processing steps were done on ice. The only modifications were that the F_c

block was incubated for 10 min, and primary antibodies were incubated for 20 min. The primary antibodies used were CD11b (M1/70) and CD45 (30F11) from BioLegend. DAPI (BD) was used as a viability stain. $DAPI^{-}CD45^{int/+}$ events were sorted on a BD FACSAria II using an 85-micron nozzle. Each sample took approximately 3-7 minutes to sort. Throughout the protocol, samples were kept on ice, and the FACSAria II was operated in a 4°C environment. In our preliminary experiments, we identified over 85% viability with this method (data not shown). The samples were immediately processed for single-cell capture as described below.

Single-cell Sequencing

Cellular suspensions containing 50,000-90,000 $CD45^{int/+}$ events were loaded on a Chromium Single-Cell Instrument (10x Genomics, Pleasanton, CA, USA) to generate single-cell Gel Bead-in-Emulsions (GEMs). Single-cell RNA-Seq libraries were prepared using Chromium Next GEM Single Cell 3' GEM, Library & Gel Bead Kit v3.1 (10x Genomics). The beads were dissolved, and cells were lysed per the manufacturer's recommendations. GEM reverse transcription (GEM-RT) was performed to produce a barcoded, full-length cDNA from poly-adenylated mRNA. After incubation, GEMs were broken, and the pooled post-GEM-RT reaction mixtures were recovered, and cDNA was purified with silane magnetic beads (DynaBeads MyOne Silane Beads, PN37002D, ThermoFisher Scientific). The entire purified post GEM-RT product was amplified by PCR. This amplification reaction generated sufficient material to construct a 3' cDNA library. Enzymatic fragmentation and size selection was used to optimize the cDNA amplicon size, and indexed sequencing libraries were constructed by End Repair, A-tailing, Adaptor Ligation, and PCR. Final libraries contain the P5 and P7 priming sites used in Illumina bridge amplification. Sequence data were generated using Illumina's NovaSeq 6000.

scRNAseq Data Analysis

CellRanger v3.1.0 pipeline was used to demultiplex, make fastq files and generate gene counts of expression data referenced to mm10-3.0.0. It was determined that pooled samples had 150,000-200,000 mean reads per cell. Over 95% of reads were mapped to the genome, and over 93% of reads were above the quality control score of Q30. The gene expression matrix was analyzed by Seurat v3.1.5 package. Genes detected in less than 3 cells, and ribosomal genes were excluded from the analysis. Cells expressing less than 200 unique genes/features, more than mean+3*standard deviation number of transcripts, or more than 5% mitochondrial genes were excluded from the analysis. Overall, this approach yielded 5943 cells for 3xTg control-chow group and 9885 cells for the 3xTg PLX-repopulated group. These two groups of cells were further compared for findings reported in the main figures. In Supplemental data, we also show a direct comparison of these two groups to the 4979 cells identified from the non-transgenic (NTg) group.

Following the above filtering criteria, the data was normalized, 2000 most variable features were selected, and their expression was scaled with the built-in functions of the Seurat package. The top 20 Principal Components (PCs) were used for subsequent clustering (resolution = 0.25) and UMAP dimension reduction. To directly compare 3xTg microglia with NTg microglia, we used the anchoring algorithm of the Seurat package since these mouse lineages are bred to homozygosity, and the mice are not littermates. No anchoring algorithm was used for comparisons between control and PLX-repopulated 3xTg microglia. The scMCA package was used for the initial annotation of the cells (39). The clusters encompassing perivascular macrophages and microglia (PVMMicro) were manually annotated according to the list of differentially expressed features that were determined by the FindMarkers() function with default Wilcoxon rank-sum test and |logFC| > 0.25. Significantly (padj < 0.05), up-and down-regulated features were used as input to ClusterProfiler v3.16.0 for overrepresentation analysis to identify significantly enriched gene sets. FindMarkers() function was also used to identify differentially expressed features between the two chow treatments.

In situ hybridization

PFA-fixed brain slices were used for *in situ* hybridization. RNAScope multiplex V2 Assay (ACD Bio) was used to detect *Cxcl13* (ACD Bio, 406311) transcripts per manufacturer's instructions with slight modifications. Specifically, tissue mounted on SuperFrost Plus slides (Fisher Scientific) was subjected to 5 min of antigen retrieval at ~100°C and was digested for 30 min with Protease Plus (ACD Bio). Opal 520 dye (Akoya Biosciences) was used at 1:800 for the detection of transcripts. Negative and positive control probes and spleen tissue (data not shown) were stained in tandem with experimental samples.

ELISA and Western Blot

Frozen hippocampi were homogenized in Tissue Protein Extraction Reagent (ThermoFisher Scientific) at a concentration of 50 mg/ml with 1X Halt Protease and Phosphatase Inhibitor Single-Use Cocktail (ThermoFisher Scientific), vortexed and sonicated. The homogenates were centrifuged for 100,000xg for 1 hour. The supernatant was collected as the soluble fraction; whereas the pellet was incubated in guanidinium-HCl pH 6.0 for 4 h and centrifuged at 100,000xg for 1 hour. This new supernatant was collected as the insoluble fraction. For Aβ40 ELISAs (ThermoFisher Scientific), the soluble fraction was diluted at 1:20, and the insoluble fraction was diluted at 1:3000. For Aβ42 ELISAs (ThermoFisher Scientific), the soluble fraction was diluted 1:2, and the insoluble was diluted 1:30. The soluble fraction diluted at 1:3 was used as input to the CXCL13 ELISA kit (R&D Systems). All dilutions were established empirically.

Statistical analysis

All statistical analyses were performed in Graphpad Prism v7.04. Comparisons between PLX and control-treated groups in male-only experiments were made using Student's t-test. Comparisons of MeX04 and MFI of several homeostatic markers were made using two-way ANOVA with Bonferroni correction. All data points that represent individual animal averages are presented as mean ± SEM. * $p < 0.05$, ** $p < 0.01$, *** $p < 0.001$.

Results

Pharmacologically-induced microglial self-renewal does not ameliorate amyloid pathology or neuritic damage in 3xTg and APP/PS1 mouse models

To explore the impact of microglia self-renewal on AD pathology, we utilized an established paradigm that partially depletes microglia using PLX5622 (PLX), a Colony Stimulating Factor 1 Receptor (CSF1R/c-kit/Flt3) inhibitor, in 3xTg and APP/PS1 mouse models of AD. After 2 weeks of PLX exposure, microglia numbers in the brains of aged (14-month-old) APP/PS1 mice decreased by approximately 65% (Supplemental Figure 1A-B). Consistent with previous findings (19), we observed greater depletion in plaque-devoid regions (70%) versus 50% depletion of plaque-associated microglia (Supplemental Figure 1C-D). The impact of microglial repopulation was assessed 1 month after the discontinuation of PLX treatment (Figures 1A; 2A). We found that self-renewal of microglia did not improve amyloid pathology, evidenced by the unaltered area fraction occupied by amyloid plaques, as well as the average size and number of plaques in either male 3xTg (Figure 1C-D, F-G) or APP/PS1 mice of both sexes (Figure 2C-D and Supplemental Figure 2A-B).

Furthermore, when we examined dense-core plaques in 3xTg mice, detected with MeX04, we observed no change with microglial repopulation (Figure 1I-K). While ELISA measurements revealed a significant decrease of insoluble Aβ42, we did not detect any statistically significant changes in soluble forms of Aβ42 and Aβ40 or insoluble Aβ40 (Supplemental Figure 3A-D). Since amyloid pathology only weakly correlates with neuronal loss and cognitive function (40), we sought to examine the impact of PLX treatment on the levels of dystrophic neurites in both APP/PS1 and 3xTg mice. In contrast to our expectations, we observed no improvement in levels of neuritic damage, indicated by similar expression of LAMP1, a lysosomal membrane glycoprotein, under all conditions (Figure 1E, H; 2E), except in the subiculum of female APP/PS1 mice, where repopulation increased LAMP1 expression (Supplemental Figure 2C). Consistent with a lack of improvement in neuritic damage, microglia renewal did not lead to changes in a battery of behavioral assays, including NOR, CFC, and Lashley III maze, in 3xTg mice (Supplemental Figure 4A). Behavioral readouts for recognition, fear, spatial memory, and anxiety showed no difference in 21-month-old PLX-treated 3xTg mice when compared to control 3xTg mice (Supplemental Figure 4B-F).

Repopulated microglia exhibit no differences in their recruitment to and phagocytosis of amyloid plaques but show complex changes in the expression of activated and homeostatic markers

While microglial repopulation did not significantly attenuate plaque pathology or influence behavioral performance (Figures 1 and 2; Supplemental Figures 2, 3, and 4), we sought to determine whether repopulated microglia exhibited any changes in phagocytic potential or their expression of signature homeostatic and activation markers (Figure 3). In order to assess microglial capacity to phagocytose plaques, we injected MeX04, a brain-permeable fluorescent probe for Aβ, 24 h prior to sacrifice and FACS sorted hippocampal $CD11b^{+}CD45^{int}$ microglia into $MeX04^{+}$ and $MeX04^{-}$ fractions (Supplemental Figure 5). The percentage of $MeX04^{+}$ microglia, which represents the proportion of plaque-phagocytosing microglia, was not significantly different between PLX and control treatments, although there was a trend toward a higher fraction of microglia internalizing MeX04 with PLX treatment in the 3xTg model (3xTg: Figure 3A, p=0.14; APP/PS1: Supplemental Figure 6A and 7A). In agreement with these findings, microglia recruitment to plaque, quantified by the amount of Iba1 immunoreactivity in close proximity to plaque, also remained unaltered after repopulation (Figure 3F, J; Supplemental Figure 6E and 7E). Similarly, we did not observe changes in total microglial volume coverage (Figure 3G, K; Supplemental Figure 6D and 7D).

We next assessed the expression patterns of CD68, P2RY12, and TMEM119 in repopulated microglia (Figure 3B-C, H-I, L-M; Supplemental Figure 6B-C, G and 7B-C, F). Repopulated microglial expression of CD68, a well-known marker for reactive microglia, decreased in the subiculum of 3xTg mice (Figure 3H, p=0.06) and in the subiculum and CA1 in APP/PS1 mice, although the main effect of PLX-treatment was only statistically significant in APP/PS1 female mice (Supplemental Figure 6G and 7F). Furthermore, microglial CD68 expression was unchanged between the 3xTg groups in CA1, a region that doesn't display amyloid pathology in these mice (Figure 3I). The expression patterns of homeostatic markers P2RY12 and TMEM119 were more complex, reflecting the difference in pathologies between the two models. In the 3xTg model, the PLX treatment group expressed significantly lower levels of P2RY12 (Figure 3B) but slightly higher levels of TMEM119 (Figure 3C), albeit not significantly (p = 0.09). Due to the restricted amyloid pathology in the subiculum in 3xTg mice, the amount of $MeX04^{+}$ microglia was too small to analyze separately and, therefore, was combined with $MeX04^{-}$ microglia for analysis. Quantification of P2RY12 intensity in brain tissue revealed a similarly decreased (although not significant) expression of P2RY12 in the CA1 region of the hippocampus, a region with hyperphosphorylated Tau but lacking amyloid pathology (Figure 3M, p=0.15), but not in the subiculum, which displays amyloid pathology (Figure 3L). In the APP/PS1 model with only amyloid pathology, the expression of TMEM119 significantly increased with the repopulation of microglia in males but not in females (Supplemental Figure 6B and 7B). A similar pattern was observed with P2RY12 expression for males, which shows a trend (p = 0.15) toward higher levels with microglial repopulation (Supplemental

Figure 6C, $p_{F(treatment)} < 0.05$). As expected, MeX04^{+} microglia showed decreased expression of TMEM119 and P2RY12 compared to MeX04^{-} microglia in both sexes of APP/PS1 mice (Supplemental Figures 6B-C and 7B-C).

Repopulated microglia impact phosphorylation of different Tau epitopes

To examine the effects of repopulated microglia on Tau pathology, we quantified the levels of two different phosphorylated Tau epitopes, pT205 and pS396, in two cohorts of 3xTg mice of similar age (Figure 4A). When normalized to total Tau expression, we found that repopulation of microglia led to a significant increase in pT205 signal in the first cohort (Figure 4B) and a slight but non-significant increase in the second cohort (Figure 4D). Interestingly, levels of pS396 with respect to total Tau were unchanged in the first cohort but showed a trend for decreased expression (p=0.05) in the second cohort (Figure 4C and E).

scRNAseq reveals a microglia subset that expresses high levels of *Cxcl13* after repopulation in aged 3xTg mice

To determine transcriptomic correlates of microglial repopulation, we performed single-cell RNA sequencing (scRNAseq) of FACS isolated CD45$^{int/+}$ cells from pooled hippocampi (Figure 5A). After quality control, we identified 15,828 cells for further bioinformatic analysis. Cells identified as doublets or apoptotic were excluded as described in *Methods.* Clustering analysis through the Seurat package revealed 9 distinct clusters in our dataset, plotted on Uniform Manifold Approximation and Projection (UMAP) space, without any anchoring algorithms that may artificially coerce the position of individual data points (Figure 5B). By using the single-cell Mouse Cell Atlas (scMCA package), we identified 5 major cell types: Perivascular macrophages and microglia (PVMMicro), T cells, B cells, and neurons (Figure 5B Inset). Microglial cells represented the overwhelming majority of identified cells and were further subdivided into 6 clusters (Figure 5B-D).

In our dataset, most cells were identified as homeostatic microglia (Figure 5C). These cells expressed markers such as *P2ry12*, *Cxc3cr1,* and *Tmem119* (Figure 5D). The second most abundant cell type observed in both groups resembled Activated Response Microglia (ARMs; or Disease-Associated Microglia, DAM). This well-established cluster was identified based on the expression of *Tyrobp*, *Apoe*, *Lpl*, *Cst7,* and other markers in accordance with previous research (Figure 5D) (3, 4, 14, 41). Similarly, we identified a cluster enriched in interferon-related genes such as *Ifitm3* and *Isg15* (Figure 5D). We believe these cells might be related to interferon response microglia (IRMs) which have also been previously observed (14). We also observed a small cluster of microglial cells with high expression levels of cell cycle and DNA replication genes, such as *Mki67* (Figure 5B, D), which could represent dividing microglia (“div mg”, also known as Cycling / Proliferating microglia or CPM). This small cluster has been identified

in previous scRNAseq studies, too (14). Together, these four clusters accounted for a similar proportion of total cells between control and repopulated microglia (Figure 5C).

Furthermore, between 3-5% of $CD45^{int/+}$ cells in the hippocampus fell into a microglial cluster defined by downregulation of cytoskeletal genes such as *Actb* (translates to β-actin) and *Tuba1b*; but also by upregulation of the long non-coding RNA *Malat1* (Figure 5D). Gene Ontology analysis through clusterProfiler revealed that genesets pertinent to the regulation of actin, as well as mitochondrial function, were negatively enriched (Supplemental Figure 9A-B). This cluster, which we refer to as "cyto-mg" for the purposes of this study, was found in similar proportions between control and PLX-repopulated (4.5% and 3.4%, respectively) groups but in much higher proportions in NTg mice (24.6%, Supplemental Figure 10A-C).

Lastly, we identified a cluster ("PLX-microglia") whose proportion changed between 3xTg control-treated and PLX-repopulated microglia (Figure 5B). This "PLX-microglia" cluster made up 12.1% of $CD45^{int/+}$ cells in the PLX-repopulated group but only 2.3% of cells in control-treated group in 3xTg mice (Figure 5C). The PLX-microglia cluster was very strongly and almost exclusively (|logFC threshold| > 1.9, Supplemental Table 1), characterized by upregulation of *Cxcl13* (Figure 5E). Detailed analysis of all microglial clusters revealed that PLX-repopulated microglia expressed more *Cxcl13* in general (Figure 5E and Supplemental Table 1). In contrast, *Cxcl13* was detected in very few microglia isolated from control treated NTg mice (Supplementary Figure 10D). We confirmed increased CXCL13 expression in hippocampal lysates through ELISA (Figure 5F), and we visualized *Cxcl13* mRNA expression through RNAScope technology (Figure 5G). We found strong trends towards increased *Cxcl13* expression in CA1 (p=0.05) and subiculum (p=0.06) in PLX-repopulated mice compared to the controls (Figure 5H-I), but there was no meaningful difference between the groups in the cortex (p=0.64, Figure 5J).

Discussion

In this present study, we investigated the impact of pharmacologically-induced microglial renewal on pathology, microglial activation, and gene expression using both the 3xTg and APP/PS1 mouse models of Alzheimer's disease. Previous work from our laboratory and others demonstrated that adult microglia are capable of rapid self-renewal following depletion (26, 42). These new-born microglia are thought to be "rejuvenated" and beneficial in the context of disease settings such as toxin-induced acute neuronal lesion as well as normal aging (28, 29). However, despite the emerging clinical relevance of targeting the neuroimmune system in AD patients (43), the long-term effects of microglial repopulation in the context of advanced-stage Alzheimer's disease have not been fully explored. Here, we demonstrated that two weeks of microglial depletion (which depleted more than 50% of the microglial population) followed by one month of microglial repopulation did not change amyloid pathology or levels of dystrophic neurites. However, we observed complex changes in Tau pathology and microglial activation markers. In addition, we identified a novel subpopulation of microglia enriched in the PLX-repopulated 3xTg microglia, which to the best of our knowledge, has not been described before.

Repopulated microglia do not ameliorate amyloid pathology but exhibit complex changes in activated and homeostatic markers in 3xTg and APP/PS1 mice

While microglia have complex roles in AD pathology, several studies have shown the benefits of eliminating microglia in AD mouse models. Although prolonged PLX treatment did not alter plaque load or Aβ levels in either 5xFAD (4-week PLX treatment starting at 14-month) (19) or 3xTg mice (12-week PLX treatment starting at 15-month) (18), both studies found that chronic microglial elimination partially prevented cognitive dysfunction in these mice (18, 19), suggesting microglia contribute to neuronal dysfunction possibly via release of inflammatory cytokines and chemokines in the chronic neuroinflammatory environment (19). Thus, “rejuvenating” microglia by pharmacologically inducing their repopulation could replace these microglia that have been shaped by their prolonged residence in an inflammatory environment, resulting in new microglia that better perform homeostatic functions. However, our experiments show that microglial repopulation did not ameliorate neuritic damage or improve cognitive outcomes in old AD-like animals (Figures 1, 2 and Supplemental Figure 2). One potential explanation for our results is that the repopulated microglia after PLX-depletion are “primed” by the surrounding CNS microenvironment in the aged brain and adapt a pro-inflammatory profile rapidly after they are born (30). In fact, notwithstanding the partial reversal of age-associated changes in microglial P2RY12, TMEM119, and CD68 expression after depletion-repopulation observed in our study (Figure 3 and Supplemental Figure 6-7), other investigators have shown that repopulated microglia do not alter the response to immune challenges and that inflammation-related gene expression was similarly unchanged by repopulation in aged mice (28, 30).

Interestingly, a recent study demonstrated that PLX treatment caused a significant shift from compact to diffuse plaque morphology with increasing neuritic damage (44), contrary to the studies mentioned above. These findings support a pivotal role for microglia in limiting fibrillar plaque expansion by encapsulating Aβ to form a protective barrier, preventing toxic effects of filamentous Aβ on nearby neurons (38, 45). Disruption to microglial clustering around plaques led to a shift in plaque structure from compact to more diffuse with complex fibrillar branching, resulting in more dystrophic neurites surrounding plaques (38). However, when microglia were allowed to repopulate, amyloid pathology was comparable to that in non-depleted animals, suggesting that the repopulated microglia replaced the resident population but did not offer further disease-modifying benefits (44). This is consistent with our observation that microglial repopulation did not alter amyloid pathology or improve dystrophic neurites surrounding plaques (Figure 1, 2 and Supplemental Figure 2). Although we observed a decrease in insoluble Aβ42 measured by ELISA, the insoluble Aβ40 and the soluble fractions of both Aβ42 and Aβ40 remained unchanged (Supplemental Figure 3). Thus, our data add to previous findings and suggest no clear benefit of repopulation to amyloid pathology or cognitive outcomes (Figure 1, 2 and Supplemental Figure 2-4) in two additional AD models at stages of pathology that are relatively advanced (≥21-month 3xTg mice and 14-month APP/PS1 mice). On the other hand, chronic microglia depletion that is started before pathology onset (i.e., prior to plaque formation) led to a decrease in plaque burden and reduction

of dystrophic neurites (20, 21), suggesting that intervening before the environment becomes inflammatory may lead to better outcomes. Furthermore, it appears that simply limiting microglial proliferation also reduces pathology (46), consistent with recent findings on the critical role of microglia in amyloid plaque seeding (9). However, microglial depletion after pathology onset is more relevant to clinical settings where patients are diagnosed once their symptoms are evident.

Repopulated microglia impact phosphorylation of certain Tau epitopes

Since microglia play a complex role in the development of Tau pathology, the impact of their depletion and/or repopulation is of substantial clinical importance. The outcomes from depletion-only paradigms have revealed conflicting results depending on models used and dosages of CSF1R-antagonists administered (18-21, 47-50). However, this is the first study to our best knowledge that has characterized the impact of microglial repopulation post-depletion on a transgenic model of Tau pathology. This is an important undertaking since side effects of sustained CSF1R inhibition can lead to uncharacterized outcomes (51). We found that PLX-based repopulation of microglia increased pT205 immunopositivity, but not that of pS396 in CA1 (Figure 4). A study in 5xFAD mice, in which Tau was seeded after the depletion and repopulation phases, also found increased phospho-Tau immunoreactivity (52). In our experiments, these observations correlated with decreased P2RY12 MFI from flow cytometry measurements (Figure 3B), consistent with the notion that activated, inflammatory microglia can worsen Tau pathology (53).

Plaque-associated microglia or DAMs are resistant to CSF1R antagonist-based depletion paradigm due to activation of downstream mediators of TREM2 (54, 55). In fact, scRNAseq studies have revealed that DAM microglia are overrepresented following CSF1R antagonist mediated depletion (47). One explanation for the overall activated microglial profile characterized by P2RY12 downregulation in 3xTg mice after repopulation (Figure 3B) could be that DAM microglia, which are resistant to depletion, give rise to new microglia that then repopulate the AD brain in these mice. It would be interesting to characterize the epigenomic profiles of repopulated microglia to determine whether they share similar chromatin accessibility features with DAM. Additionally, examination of exosome release from repopulated microglia may reveal clues on whether Tau spread through exosomes (56) is implicated in our paradigm.

Transcriptomic analysis of repopulated microglia identifies novel microglial subpopulations associated with PLX treatment and 3xTg phenotype

Transcriptomic analysis of our microglial repopulation paradigm in 3xTg mice identified previously reported clusters of microglia associated with AD but also noted two distinct, previously unreported

clusters. The “Cyto-mg” cluster was similarly represented in PLX-repopulated and control 3xTg mice, but its prevalence was greatly reduced compared to the NTg control mice (Supplemental Figure 10A-B). Gene ontology analysis of downregulated transcriptomic markers that define this cluster revealed significant enrichment of gene sets pertinent to cytoskeleton organization and mitochondrion organization (Supplemental Figure 9). Interestingly, the most upregulated gene in this cluster was *Malat1* (Figure 5D, Supplemental Table 1), which has been shown to play roles in various neuroinflammatory insults – potentially through activation of the inflammasome (57). However, we also acknowledge that downregulation of aforementioned gene ontology terms (Supplemental Figure 9) may represent an artifactual outcome due to the lower number of detected RNA molecules or annotated genes (Supplemental Figure 8). Further, it is unclear whether the transcriptomic signature of “Cyto-mg” cluster exists in microglia in other models of Tau pathology. Single-cell sequencing of microglia from Thy-Tau22 mice revealed a transcriptomic landscape characterized by increased proportions of ARM (or DAM) rather than a signature associated with cytoskeletal components or *Malat1* (58). However, in that study, the authors anchor their Tau datasets with APP/PS1 datasets using CCA as a dimensionality reduction method (as opposed to PCA) which might have masked rare populations that exist only in one group (59). Nevertheless, questions pertinent to existence and/or function of “Cyto-mg” cluster in models of AD are beyond the scope of this paper.

The other previously unreported cluster that we observed here is strongly defined by upregulation of *Cxcl13* (Figure 5B, D). Although this “PLX-microglia” cluster was distinct from other types of activated microglia, we also observed *Cxcl13* upregulation in Homeo and ARM/DAM clusters, which account for most of the microglia, but not in other $CD45^{int/+}$ cells (Figure 5C, E and Supplemental Table 1). As expected, statistical testing on all cells identified as microglia revealed significant upregulation of *Cxcl13* in PLX-treated groups (Supplemental Table 1). Furthermore, we were able to confirm this finding at the protein level (Figure 5F). Interestingly, we observed strong trends towards upregulation of *Cxcl13* transcripts with *in situ* hybridizations in CA1 and subiculum of PLX-repopulated mice, but this effect was not detected in the cortex (Figure 5H-J). This may suggest that *Cxcl13* is expressed in regions that display AD pathology. Since CXCL13 plays an important role in homing and activation of $CXCR5^{+}$ lymphocytes, such as B cells, follicular helper T cells, and Th17 cells (33), this transcriptomic signature might suggest an overall increased inflammatory environment. This is further supported by decreased microglial expression of P2RY12 (Figure 3B). CXCL13 expression has also been observed in models of MS, particularly in CSF and meningeal tertiary lymphoid organs (31). Whether this leads to increased lymphocyte infiltration or formation of tertiary lymphoid organs following microglial repopulation in AD mouse models warrants further research.

Lastly, we found similar proportions of DAM/ARM between control and repopulated groups in 3xTg mice. This finding contrasts another study (52) in which microglia did not re-establish DAM signature following a repopulation paradigm in the 5xFAD model. Although it is difficult to directly compare across studies due to the use of different sequencing technologies that provide different levels of resolution (microarray vs scRNAseq), we argue that the age of animals (~5 months vs. 23 months), as well as the presence of

active Tau pathology in our model, may have created an environment that is conducive to re-establishment of the DAM/ARM signature.

Concluding Remarks

Taken altogether, we provide evidence that depleting and repopulating the microglia in the context of ongoing simultaneous amyloid and tau pathologies can increase hyperphosphorylation of specific isoforms of Tau despite having no apparent effect on Aβ plaque load. This effect on pathology correlated with increased reactivity of microglia in the hippocampus as characterized by decreased expression of homeostatic markers. Furthermore, microglial repopulation led to the emergence of a microglial subpopulation that strongly expresses *Cxcl13*. This signature was spatially associated with regions of pathology in the 3xTg mouse model.

Abbreviations

AD: Alzheimer's disease; CNS: Central nervous system; OF: Open field; CFC: Contextual fear conditioning; NOR: Novel object recognition; Aβ: amyloid beta; ELISA: Enzyme-linked immunosorbent assay; MeX04: Methoxy-04; CSF1R: Colony Stimulating Factor 1 Receptor; pS396: phosphorylated Tau at Serine 396; pT206: phosphorylated Tau at Threonine 206; scRNAseq: single-cell RNA sequencing; DAM: Disease associated microglia; ARM: Activated response microglia; IRM: Interferon response microglia; *Cxcl13*: C-X-C Motif Chemokine Ligand 13; P2RY12: Purinergic Receptor P2Y12; TMEM119: Transmembrane Protein 119.

Declarations

Ethical approval and consent to participate

This animal study was reviewed and approved by the University Committee on Animal Resources of the University of Rochester Medical Center.

Consent for publication

Not applicable.

Availability of data and materials

The raw data supporting the conclusions of this article will be made available by the authors, without undue reservation, to any qualified researcher upon request. The sequencing dataset supporting the conclusions of this article is available in Gene Expression Omnibus repository under accession number GSE190607.

Competing interests

The authors declare that they have no competing interests.

Funding

This research was supported by Alzheimer's Association grant AARG-NTF-19-619116, University of Rochester Medical Center's Del Monte Institute for Neuroscience Pilot Program, and NIH grants R01 AG030149, R01 NS114480-2W2, R56 AG066397, and F99 NS108486-02.

Authors' contributions

BK and MSM conceived the study in consultation with AKM and MKO. BK, LL, and MSM conducted all experiments, carried out all data analyses, and wrote initial drafts of the manuscript. All authors reviewed and contributed to the final version.

Acknowledgments

We thank Lee Trojanczyk, Joshua Boyer, and Laura Owlett for technical assistance with tissue procurement and processing. We thank the staff of Center for Advanced Light Microscopy and Nanoscopy (CALMN; University of Rochester Medical Center) for image acquisition discussions. We also thank the Flow Cytometry Core (FCC; University of Rochester Medical Center) for technical assistance. We thank the Genomics Research Center (GRC; University of Rochester Medical Center) for processing samples and running the 10X Chromium scRNASeq pipeline. We thank the bioinformatics team at GRC and are particularly grateful for the assistance of Dr. Andrew McDavid and Dr. Matthew N. McCall for their guidance and suggestions in interpreting scRNAseq data. Lastly, we thank Dr. Alison Elder for providing the 3xTg and NTg mice used in this study.

References

1. Heneka MT, Carson MJ, El Khoury J, Landreth GE, Brosseron F, Feinstein DL, et al. Neuroinflammation in Alzheimer's disease. Lancet Neurol. 2015;14(4):388-405.
2. Hardy J, Selkoe DJ. The amyloid hypothesis of Alzheimer's disease: progress and problems on the road to therapeutics. Science. 2002;297(5580):353-6.
3. Butovsky O, Weiner HL. Microglial signatures and their role in health and disease. Nat Rev Neurosci. 2018;19(10):622-35.
4. Keren-Shaul H, Spinrad A, Weiner A, Matcovitch-Natan O, Dvir-Szternfeld R, Ulland TK, et al. A Unique Microglia Type Associated with Restricting Development of Alzheimer's Disease. Cell. 2017;169(7):1276-90 e17.

5. Butovsky O, Jedrychowski MP, Moore CS, Cialic R, Lanser AJ, Gabriely G, et al. Identification of a unique TGF-beta-dependent molecular and functional signature in microglia. Nat Neurosci. 2014;17(1):131-43.
6. Hammond TR, Dufort C, Dissing-Olesen L, Giera S, Young A, Wysoker A, et al. Single-Cell RNA Sequencing of Microglia throughout the Mouse Lifespan and in the Injured Brain Reveals Complex Cell-State Changes. Immunity. 2019;50(1):253-71 e6.
7. Li Q, Cheng Z, Zhou L, Darmanis S, Neff NF, Okamoto J, et al. Developmental Heterogeneity of Microglia and Brain Myeloid Cells Revealed by Deep Single-Cell RNA Sequencing. Neuron. 2019;101(2):207-23 e10.
8. Krasemann S, Madore C, Cialic R, Baufeld C, Calcagno N, El Fatimy R, et al. The TREM2-APOE Pathway Drives the Transcriptional Phenotype of Dysfunctional Microglia in Neurodegenerative Diseases. Immunity. 2017;47(3):566-81 e9.
9. Huang Y, Happonen KE, Burrola PG, O'Connor C, Hah N, Huang L, et al. Microglia use TAM receptors to detect and engulf amyloid beta plaques. Nat Immunol. 2021;22(5):586-94.
10. Prasad H, Rao R. Amyloid clearance defect in ApoE4 astrocytes is reversed by epigenetic correction of endosomal pH. Proc Natl Acad Sci U S A. 2018;115(28):E6640-E9.
11. Atagi Y, Liu CC, Painter MM, Chen XF, Verbeeck C, Zheng H, et al. Apolipoprotein E Is a Ligand for Triggering Receptor Expressed on Myeloid Cells 2 (TREM2). J Biol Chem. 2015;290(43):26043-50.
12. Hashimoto T, Serrano-Pozo A, Hori Y, Adams KW, Takeda S, Banerji AO, et al. Apolipoprotein E, especially apolipoprotein E4, increases the oligomerization of amyloid beta peptide. J Neurosci. 2012;32(43):15181-92.
13. Bailey CC, DeVaux LB, Farzan M. The Triggering Receptor Expressed on Myeloid Cells 2 Binds Apolipoprotein E. J Biol Chem. 2015;290(43):26033-42.
14. Sala Frigerio C, Wolfs L, Fattorelli N, Thrupp N, Voytyuk I, Schmidt I, et al. The Major Risk Factors for Alzheimer's Disease: Age, Sex, and Genes Modulate the Microglia Response to Abeta Plaques. Cell Rep. 2019;27(4):1293-306 e6.
15. Owlett LD, Karaahmet B, Le L, Belcher EK, Dionisio-Santos D, Olschowka JA, et al. Gas6 induces inflammation and reduces plaque burden but worsens behavior in a sex-dependent manner in the APP/PS1 model of Alzheimer's disease. J Neuroinflammation. 2022;19(1):38.
16. Mathys H, Adaikkan C, Gao F, Young JZ, Manet E, Hemberg M, et al. Temporal Tracking of Microglia Activation in Neurodegeneration at Single-Cell Resolution. Cell Rep. 2017;21(2):366-80.
17. Han J, Harris RA, Zhang XM. An updated assessment of microglia depletion: current concepts and future directions. Mol Brain. 2017;10(1):25.
18. Dagher NNea. Colony-stimulating factor 1 receptor inhibition prevents microglial plaque association and improves cognition in 3xTg-AD mice. Journal of Neuroinflammation. 2015;12.
19. Spangenberg EE, Lee RJ, Najafi AR, Rice RA, Elmore MR, Blurton-Jones M, et al. Eliminating microglia in Alzheimer's mice prevents neuronal loss without modulating amyloid-beta pathology. Brain. 2016;139(Pt 4):1265-81.

20. Spangenberg E, Severson PL, Hohsfield LA, Crapser J, Zhang J, Burton EA, et al. Sustained microglial depletion with CSF1R inhibitor impairs parenchymal plaque development in an Alzheimer's disease model. Nat Commun. 2019;10(1):3758.
21. Sosna J, Philipp S, Albay R, 3rd, Reyes-Ruiz JM, Baglietto-Vargas D, LaFerla FM, et al. Early long-term administration of the CSF1R inhibitor PLX3397 ablates microglia and reduces accumulation of intraneuronal amyloid, neuritic plaque deposition and pre-fibrillar oligomers in 5XFAD mouse model of Alzheimer's disease. Mol Neurodegener. 2018;13(1):11.
22. Zhao R, Hu W, Tsai J, Li W, Gan WB. Microglia limit the expansion of beta-amyloid plaques in a mouse model of Alzheimer's disease. Mol Neurodegener. 2017;12(1):47.
23. Huang Y, Xu Z, Xiong S, Qin G, Sun F, Yang J, et al. Dual extra-retinal origins of microglia in the model of retinal microglia repopulation. Cell Discov. 2018;4:9.
24. Zhan L, Krabbe G, Du F, Jones I, Reichert MC, Telpoukhovskaia M, et al. Proximal recolonization by self-renewing microglia re-establishes microglial homeostasis in the adult mouse brain. PLoS Biol. 2019;17(2):e3000134.
25. Zhang Y, Zhao L, Wang X, Ma W, Lazere A, Qian HH, et al. Repopulating retinal microglia restore endogenous organization and function under CX3CL1-CX3CR1 regulation. Sci Adv. 2018;4(3):eaap8492.
26. Mendes MS, Le L, Atlas J, Brehm Z, Ladron-de-Guevara A, Matei E, et al. The role of P2Y12 in the kinetics of microglial self-renewal and maturation in the adult visual cortex in vivo. Elife. 2021;10.
27. Askew Kea. Coupled Proliferation and Apoptosis Maintain the Rapid Turnover of Microglia in the Adult Brain. Cell Rep. 2017;18(2):391-405.
28. Elmore MRP, Hohsfield LA, Kramar EA, Soreq L, Lee RJ, Pham ST, et al. Replacement of microglia in the aged brain reverses cognitive, synaptic, and neuronal deficits in mice. Aging Cell. 2018;17(6):e12832.
29. Rice RA, Pham J, Lee RJ, Najafi AR, West BL, Green KN. Microglial repopulation resolves inflammation and promotes brain recovery after injury. Glia. 2017;65(6):931-44.
30. O'Neil SM, Witcher KG, McKim DB, Godbout JP. Forced turnover of aged microglia induces an intermediate phenotype but does not rebalance CNS environmental cues driving priming to immune challenge. Acta Neuropathol Commun. 2018;6(1):129.
31. Lalor SJ, Segal BM. Lymphoid chemokines in the CNS. J Neuroimmunol. 2010;224(1-2):56-61.
32. Kazanietz MG, Durando M, Cooke M. CXCL13 and Its Receptor CXCR5 in Cancer: Inflammation, Immune Response, and Beyond. Front Endocrinol (Lausanne). 2019;10:471.
33. Londono AC, Mora CA. Role of CXCL13 in the formation of the meningeal tertiary lymphoid organ in multiple sclerosis. F1000Res. 2018;7:514.
34. Bressler A, Blizard D, Andrews A. Low-stress route learning using the Lashley III maze in mice. J Vis Exp. 2010(39).

35. Matousek SB, Hein AM, Shaftel SS, Olschowka JA, Kyrkanides S, O'Banion MK. Cyclooxygenase-1 mediates prostaglandin E(2) elevation and contextual memory impairment in a model of sustained hippocampal interleukin-1beta expression. J Neurochem. 2010;114(1):247-58.
36. Rivera-Escalera F, Pinney JJ, Owlett L, Ahmed H, Thakar J, Olschowka JA, et al. IL-1beta-driven amyloid plaque clearance is associated with an expansion of transcriptionally reprogrammed microglia. J Neuroinflammation. 2019;16(1):261.
37. Klunk WE, Bacskai BJ, Mathis CA, Kajdasz ST, McLellan ME, Frosch MP, et al. Imaging Abeta plaques in living transgenic mice with multiphoton microscopy and methoxy-X04, a systemically administered Congo red derivative. J Neuropathol Exp Neurol. 2002;61(9):797-805.
38. Yuan P, Condello C, Keene CD, Wang Y, Bird TD, Paul SM, et al. TREM2 Haplodeficiency in Mice and Humans Impairs the Microglia Barrier Function Leading to Decreased Amyloid Compaction and Severe Axonal Dystrophy. Neuron. 2016;90(4):724-39.
39. Sun H, Zhou Y, Fei L, Chen H, Guo G. scMCA: A Tool to Define Mouse Cell Types Based on Single-Cell Digital Expression. Methods Mol Biol. 2019;1935:91-6.
40. Nelson PT, Alafuzoff I, Bigio EH, Bouras C, Braak H, Cairns NJ, et al. Correlation of Alzheimer disease neuropathologic changes with cognitive status: a review of the literature. J Neuropathol Exp Neurol. 2012;71(5):362-81.
41. Deczkowska A, Keren-Shaul H, Weiner A, Colonna M, Schwartz M, Amit I. Disease-Associated Microglia: A Universal Immune Sensor of Neurodegeneration. Cell. 2018;173(5):1073-81.
42. Elmore MR, Najafi AR, Koike MA, Dagher NN, Spangenberg EE, Rice RA, et al. Colony-stimulating factor 1 receptor signaling is necessary for microglia viability, unmasking a microglia progenitor cell in the adult brain. Neuron. 2014;82(2):380-97.
43. Cummings J, Lee G, Zhong K, Fonseca J, Taghva K. Alzheimer's disease drug development pipeline: 2021. Alzheimers Dement (N Y). 2021;7(1):e12179.
44. Casali BT, MacPherson KP, Reed-Geaghan EG, Landreth GE. Microglia depletion rapidly and reversibly alters amyloid pathology by modification of plaque compaction and morphologies. Neurobiol Dis. 2020;142:104956.
45. Condello Cea. Microglia constitute a barrier that prevents neurotoxic protofibrillar Abbeta42 hotspots around plaques. Nature communications. 2015.
46. Hu Y, Fryatt GL, Ghorbani M, Obst J, Menassa DA, Martin-Estebane M, et al. Replicative senescence dictates the emergence of disease-associated microglia and contributes to Abeta pathology. Cell Rep. 2021;35(10):109228.
47. Lodder C, Scheyltjens I, Stancu IC, Botella Lucena P, Gutierrez de Rave M, Vanherle S, et al. CSF1R inhibition rescues tau pathology and neurodegeneration in an A/T/N model with combined AD pathologies, while preserving plaque associated microglia. Acta Neuropathol Commun. 2021;9(1):108.
48. Shi Y, Manis M, Long J, Wang K, Sullivan PM, Remolina Serrano J, et al. Microglia drive APOE-dependent neurodegeneration in a tauopathy mouse model. J Exp Med. 2019;216(11):2546-61.

49. Mancuso R, Fryatt G, Cleal M, Obst J, Pipi E, Monzon-Sandoval J, et al. CSF1R inhibitor JNJ-40346527 attenuates microglial proliferation and neurodegeneration in P301S mice. Brain. 2019;142(10):3243-64.
50. Clayton K, Delpech JC, Herron S, Iwahara N, Ericsson M, Saito T, et al. Plaque associated microglia hyper-secrete extracellular vesicles and accelerate tau propagation in a humanized APP mouse model. Mol Neurodegener. 2021;16(1):18.
51. Lei F, Cui N, Zhou C, Chodosh J, Vavvas DG, Paschalis EI. CSF1R inhibition by a small-molecule inhibitor is not microglia specific; affecting hematopoiesis and the function of macrophages. Proc Natl Acad Sci U S A. 2020;117(38):23336-8.
52. Gratuze M, Chen Y, Parhizkar S, Jain N, Strickland MR, Serrano JR, et al. Activated microglia mitigate Abeta-associated tau seeding and spreading. J Exp Med. 2021;218(8).
53. Ghosh S, Wu MD, Shaftel SS, Kyrkanides S, LaFerla FM, Olschowka JA, et al. Sustained interleukin-1beta overexpression exacerbates tau pathology despite reduced amyloid burden in an Alzheimer's mouse model. J Neurosci. 2013;33(11):5053-64.
54. Wang Y, Cella M, Mallinson K, Ulrich JD, Young KL, Robinette ML, et al. TREM2 lipid sensing sustains the microglial response in an Alzheimer's disease model. Cell. 2015;160(6):1061-71.
55. Zou W, Reeve JL, Liu Y, Teitelbaum SL, Ross FP. DAP12 couples c-Fms activation to the osteoclast cytoskeleton by recruitment of Syk. Mol Cell. 2008;31(3):422-31.
56. Asai H, Ikezu S, Tsunoda S, Medalla M, Luebke J, Haydar T, et al. Depletion of microglia and inhibition of exosome synthesis halt tau propagation. Nat Neurosci. 2015;18(11):1584-93.
57. Cai LJ, Tu L, Huang XM, Huang J, Qiu N, Xie GH, et al. LncRNA MALAT1 facilitates inflammasome activation via epigenetic suppression of Nrf2 in Parkinson's disease. Mol Brain. 2020;13(1):130.
58. Sierksma A, Lu A, Mancuso R, Fattorelli N, Thrupp N, Salta E, et al. Novel Alzheimer risk genes determine the microglia response to amyloid-beta but not to TAU pathology. EMBO Mol Med. 2020;12(3):e10606.
59. Butler A, Hoffman P, Smibert P, Papalexi E, Satija R. Integrating single-cell transcriptomic data across different conditions, technologies, and species. Nat Biotechnol. 2018;36(5):411-20.

Figures

Figure 1.

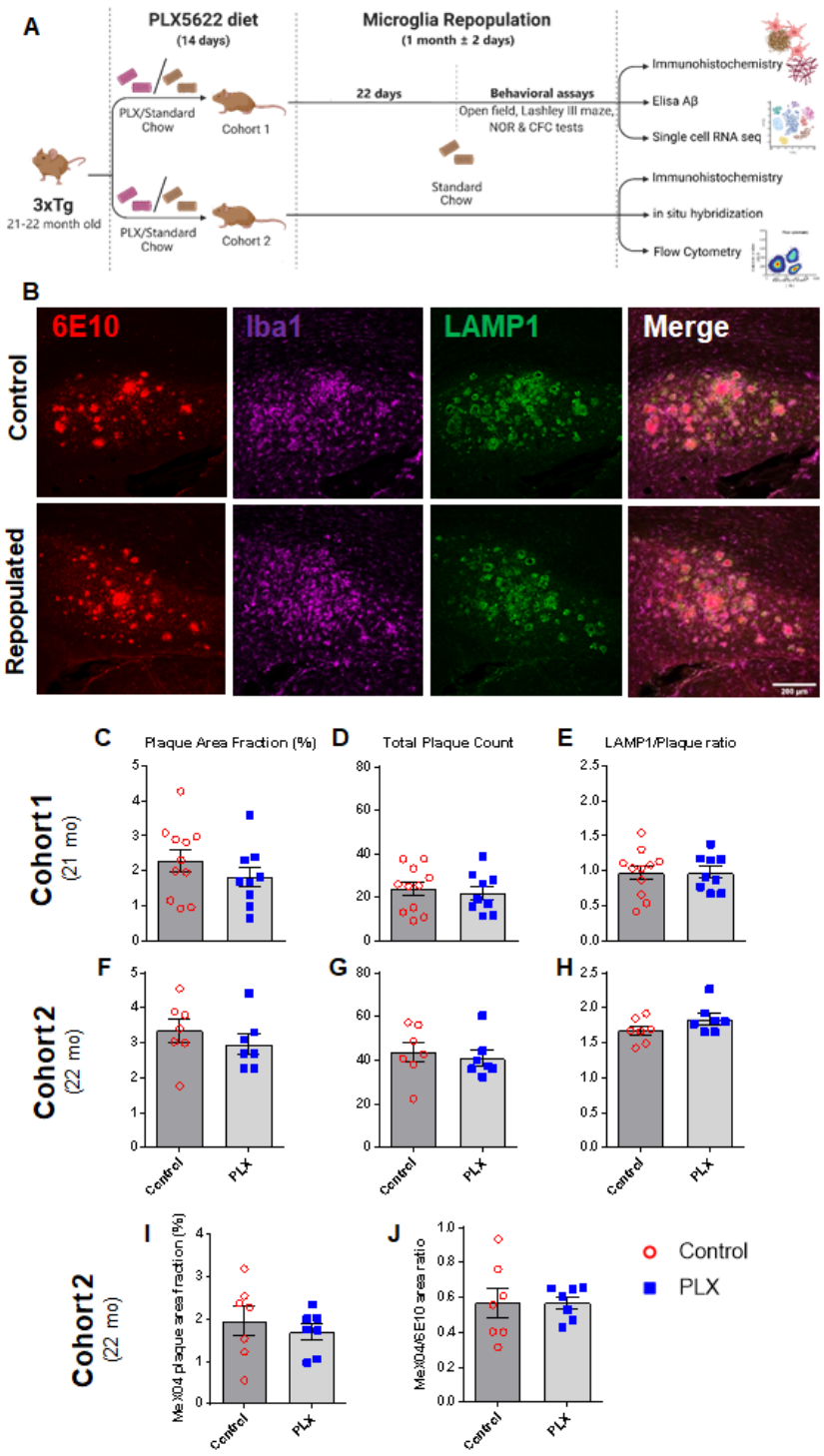

Figure 1

Repopulation of microglia does not ameliorate Aβ pathology and associated neuritic damage in 3xTg mice.

Experimental paradigm depicting duration of PLX5622 treatment and subsequent microglial repopulation (**A**). Representative confocal immunofluorescent 20x images of the subiculum in control versus PLX-

repopulated group, showing Aβ plaque (6E10, red), microglia (Iba1, magenta), neuritic damage (LAMP1, green) (**B**). Scale bar represents 200 μm. There were no significant differences in the total area (**C, F**) and number (**D, G**) of plaques between the control and PLX-repopulated group in both cohorts. Ratio of plaque-associated neuritic damage to plaque load was similar between the control and PLX-repopulated groups in both cohorts (**E, H**). There was also no difference in the total plaque area labeled with MeX04 (**I**) and the ratio of MeX04/6E10 (**J**) between the two treatment groups. Student's t-test. Data are presented as mean ± SEM (Cohort 1: n=9-11; Cohort 2: n=7)

Figure 2

Repopulation of microglia does not ameliorate Aβ pathology and neuritic damage in APP/PS1 male mice.

Experimental paradigm depicting duration of PLX5622 treatment and subsequent microglial repopulation (**A**). Representative immunofluorescent 20x images of the subiculum in control versus PLX-repopulated group, showing Aβ plaque (6E10, red), microglia (Iba1, magenta), and neuritic damage (LAMP1, green) (**B**). Scale bar represents 200 μm. There was no difference in the total area (**C**) and number (**D**) of plaques between the control and PLX-repopulated groups in Subiculum or CA1. Ratio of plaque-associated neuritic damage to plaque load was similar between control and PLX-repopulated group (**E**). Student's t-test. Data are presented as mean ± SEM (n=6)

Figure 3.

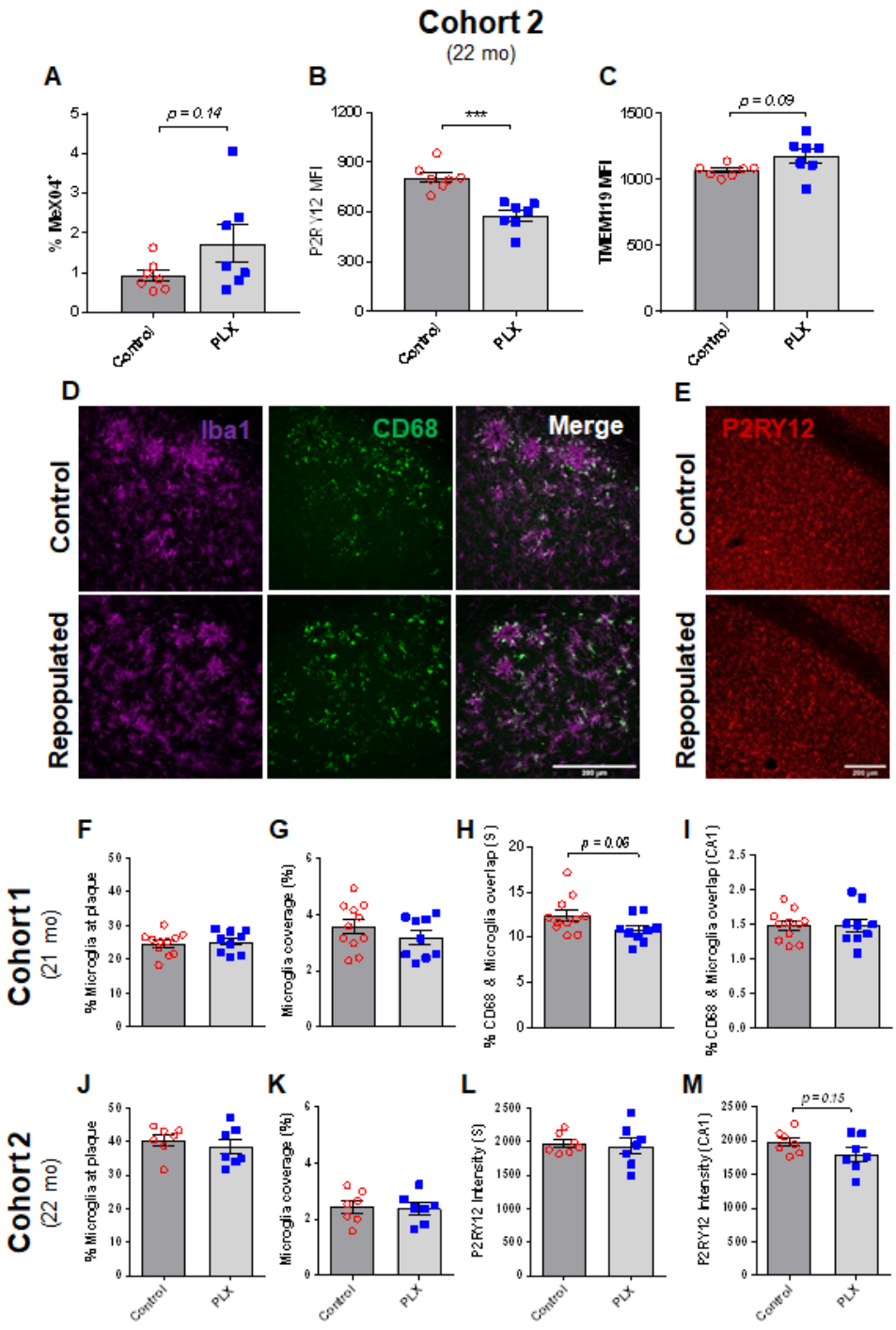

Figure 3

Repopulated microglia show similar recruitment to plaques but exhibit changes in activated and homeostatic markers.

Flow cytometry revealed no significant difference in microglia internalization of MeX04 in the two groups but a trend toward a higher percentage of MeX04^{+} microglia with PLX treatment (**A**). Microglial

expression of P2RY12 (**B**) was significantly lower, while TMEM119 expression (**C**) was mildly elevated in PLX-repopulated group compared to the control. Representative immunofluorescent 40x images of the subiculum in the control and PLX-repopulated groups showing microglia (Iba1, magenta) and CD68 (green) in the first cohort of 3xTg mice (**D**). Representative immunofluorescent 20x images of the CA1 in the control and PLX-repopulated groups showing P2RY12 (red) in the second cohort of 3xTg mice (**E**). Scale bars represent 200 µm. Microglia in both cohorts showed no difference in their recruitment to plaque (**F, J**) as well as their total volume (**G, K**) between control and PLX-repopulated groups. Expression of CD68, a marker of activated microglia, was slightly lower in the PLX-treated group in the subiculum (**H**) but not in the CA1 (**I**). The intensity of P2RY12, a homeostatic maker of microglia, was similar between treatments in the subiculum (**L**) but showed a trend toward being lower in the PLX-repopulated group in the CA1 region (**M**). Student's t-test (Welch's corrections for *A* and *C*), **** p < 0.001*. Data are presented as mean ± SEM (Cohort 1: n=9-11; Cohort 2: n=7)

Figure 4.

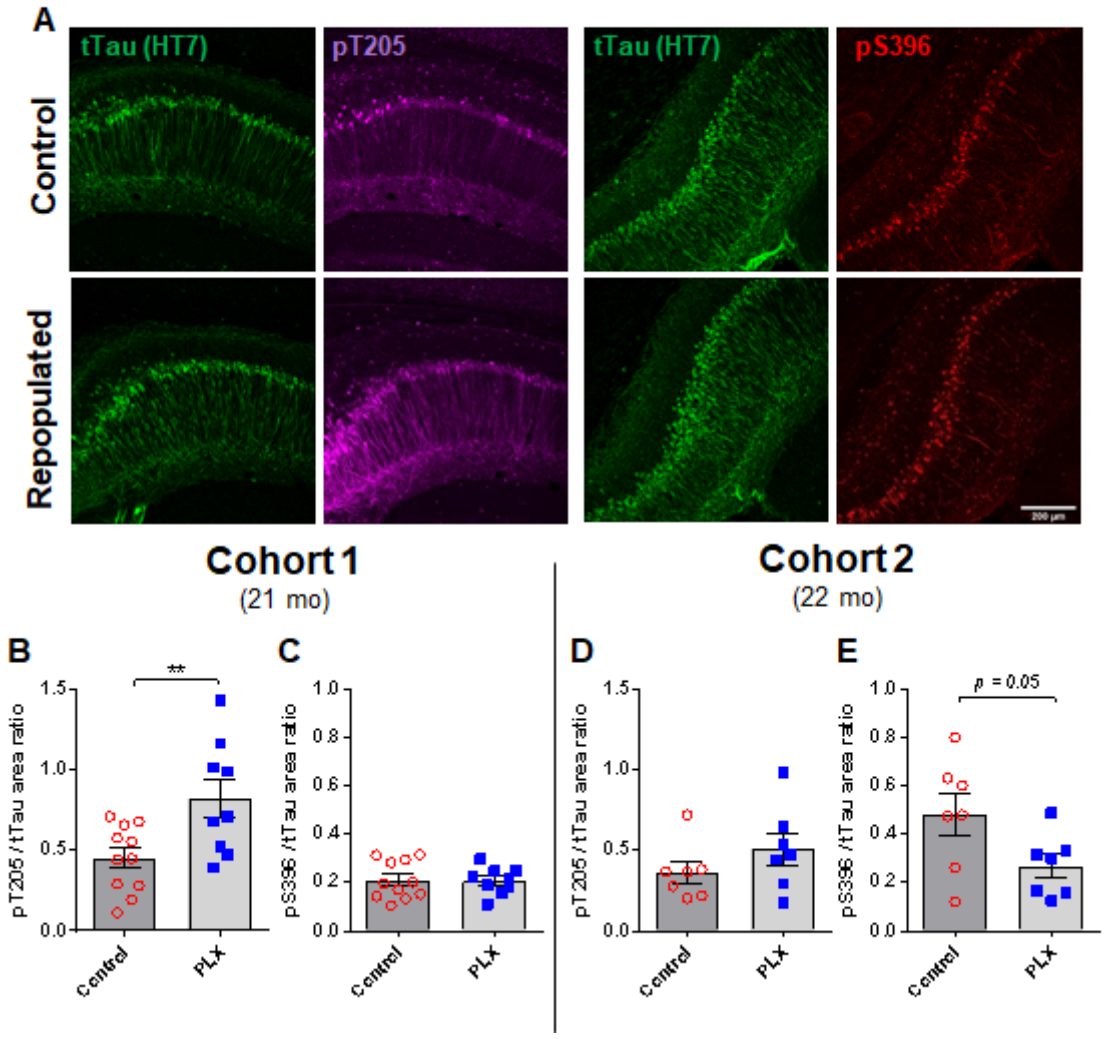

Figure 4

Repopulation of microglia impacts phosphorylation of different Tau epitopes in 3xTg mice.

Representative immunofluorescent 20x images of the CA1 hippocampal region in control and PLX-repopulated groups showing total Tau (HT7, green), pT205 (magenta), and pS396 (red) (**A**). Scale bar represents 200 µm. Quantification of pT205 revealed a significant increase in the PLX-repopulated group of Cohort 1 (**B**) but not Cohort 2 (**D**). Levels of pS396 were unchanged between control and PLX-repopulated groups of Cohort 1 (**C**), but showed a trend towards decreased expression in PLX-repopulated group of Cohort 2 (**E**). Student's t-test, *$* p < 0.05$*. Data are presented as mean ± SEM (Cohort 1: n=9-11; Cohort 2: n=7)

Figure 5

Repopulation increases *Cxcl13* expression in hippocampal microglia of 3xTg male mice.

Schematic of experimental design (**A-B**). FACS-sorted cells were used as the input for scRNAseq (**A**). UMAP plots of control and PLX-repopulated groups illustrate clustering of cells (**B**). The inset shows the output of scMCA-based cell annotations. An overwhelming majority of sequenced cells were microglia (**B**). Proportions of different cell clusters out of all sequenced cells are depicted in (**C**). Panel of genes identified through Seurat's statistical framework or established literature is shown in (**D**) for annotation purposes. Red boxes highlight genes that are associated with their corresponding clusters. Increased *Cxcl13* expression can be noted across the majority of repopulated microglia but in particular for PLX-mg and ARM/DAM clusters (**E**). Increasing tones of green denote increased *Cxcl13* expression. ELISA on hippocampal lysates confirmed the upregulation of Cxcl13 at the protein level (**F**). Representative immunofluorescent 10x images of *in situ* analysis of *Cxcl13* expression (**G**). Scale bar represents 200 µm. *Cxcl13* staining showed strong trends towards increased expression in PLX-repopulated groups in Subiculum and CA1 (**H-I**), however did not change in the cortex (**J**). Student's t-test *(F, H-J), * $p < 0.05$*. Data are presented as mean ± SEM.

Supplementary Files

This is a list of supplementary files associated with this preprint. Click to download.

- KaraahmetSupplementalFigures.pptx
- SupplementalTable1.xlsx